Micromanipulation of sonoluminescing bubbles

Joachim Holzfuss and Matthias Rüggeberg
Institut für Angewandte Physik, TU Darmstadt, Schloßgartenstrasse 7, 64289 Darmstadt, Germany
(Received 16 July 2003; revised manuscript received 14 October 2003; published 18 May 2004)

Micromanipulation of sonoluminescing bubbles is achieved by generating a complex sound field consisting of spatially distributed modes of higher harmonics of a basic driving frequency. Bubbles can be manipulated in space and shifted to any desired spot. The interaction with the complex sound field also allows for specification of the violence of a bubble collapse.

DOI: 10.1103/PhysRevE.69.056304 PACS number(s): 78.60.Mq, 43.25.+y, 05.45.−a

I. INTRODUCTION

During single bubble sonoluminescence (SBSL) a bubble levitated in a fluid is oscillating violently in response to a high amplitude driving ultrasound field and emitting short light pulses at collapse time [1–3]. During this process mechanical (acoustic) energy is focused near the bubble driving it to emit a broad spectrum of photons with peak energies exceeding 3 eV. Compared to the mechanical work exerted on a single molecule by the driving circuitry, this represents an energy amplification of 13 orders of magnitude. Experiments and numerical work stimulated by speculations, whether it may be possible to further increase the violence of the collapse with the help of a modified sound field, have been used [4–12]. Two concepts have been reported: One deals with the addition of higher harmonics with a certain adjustable phase difference of a basic driving frequency [4–10], the other with the addition of pulsed ultrasound [6,11,12]. In most reports a severalfold increase of the emitted light intensity has been observed under certain experimental conditions and chosen driving parameter values. In this investigation we report on the effects of multifrequency driving of sonoluminescing bubbles under varying driving parameters, such as number of harmonics, phase, and amplitude. It is shown that parameter changes cannot only control the intensity of the collapse but also allow for spatial micromanipulation of the levitation spot of the bubble. Micromanipulation is useful in further attempts to target the bubble into the very center of a converging ultrasonic pulse [6,12] or self-generated reflected shock wave. In Ref. [13] it has been shown that during SBSL bubble collapse a shock wave is emitted from the bubble into the liquid. The side walls of the SBSL resonator cell reflect the arriving pressure pulse and aid to refocus it to a spot whereby the pulse increases its amplitude generating a shock wave. As this reflected shock may not hit the bubble at its minimal focus, spatial manipulations to the bubble could be applied to achieve spatial coincidence. Otherwise, spatial dislocations [6] may result as a consequence of a nonisotropic pressure pulse.

II. NUMERICAL MODEL

In the experiment [1] a single bubble is levitated in a standing wave sound field set up in a water column. As the bubble interacts with the sound multiple forces act on it. It is levitated with the help of the primary Bjerknes force

$$F_B = -\langle V(t)\,\nabla\, p_e(r,z,t)\rangle_t \tag{1}$$

acting on the oscillating volume $V(t)$ of the bubble. When F_B is large enough to overcome the buoyancy force

$$F_g = \langle(\rho_l - \rho_g)V(t)(9.81)\rangle_t, \tag{2}$$

with ρ_l, ρ_g, the respective liquid and bubble gas densities, the bubble is attracted to a fixed position in the fluid. The sound pressure $p_e(r,z,t)$ is a standing wave with cylindrical coordinates r, z. At moderate driving with frequencies below their linear resonance, a bubble is attracted towards the pressure antinode to a position slightly above the pressure antinode, at which the buoyant and the Bjerknes force balance. Figure 1 visualizes the behavior of a bubble of 4 μm ambient radius in a one-dimensional (1D) sound field. Omitting the r dependence, the sound field describing our experimental setup [5] is approximated as

$$p_e(z,t) = p_{e,1}\cos(\omega_1 t)\cos(k_1 z), \tag{3}$$

with $p_{e,1}=1.4$ bars, $\omega_1 = 2\pi f$, $f=23.4$ kHz, and $k_1 = 2\pi/2\lambda$, λ being the wavelength in water. The special value of the

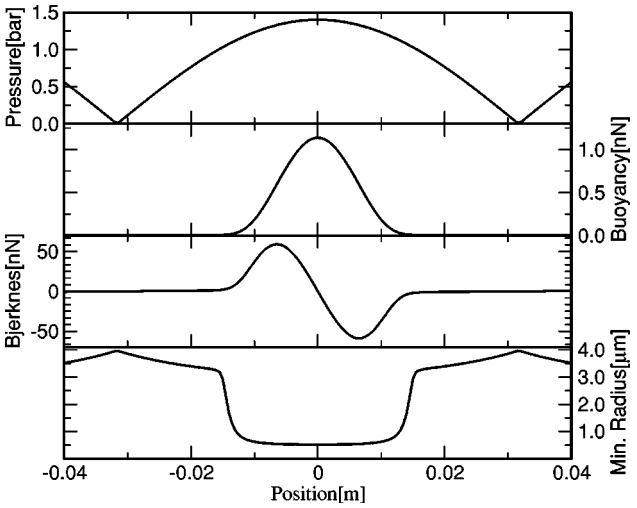

FIG. 1. Driving pressure, buoyancy force, Bjerknes force, and minimal radius at collapse of a bubble with a fixed radius of 4 μm oscillating in a vertical 1D standing wave field as a function of position using Eqs. (1)–(5).

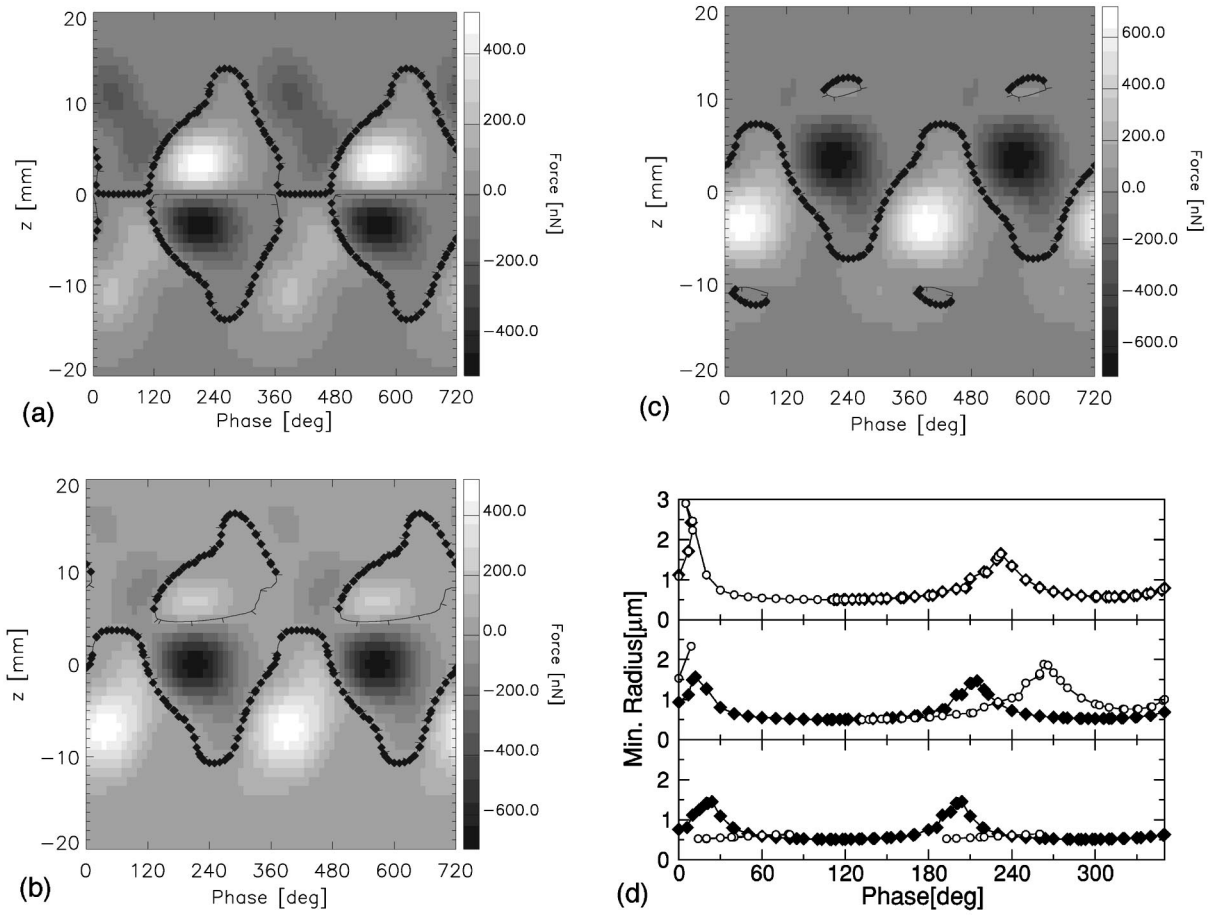

FIG. 2. Gray scale diagrams of the sum of Bjerknes and buoyancy forces on a bubble driven by a two-frequency sound field consisting of first and second harmonic. Stable and unstable positions of the bubble are shown as a function of temporal phase difference between both driving components. The driving pressure of the first harmonic ($f=23.4$ kHz) is 1.35 bars and the pressure of the second harmonic is 0.371 bars. The phase differences of the spatial modes are (a–c) 0°, −45° and −90°. (d) Minimal radii at collapse of the data in (a–c) (top to bottom). Results of the bottom stability lines have filled symbols; upper lines and islands are opaque.

wave number k_1 is reflecting the experimentally observed mode. In Fig. 1 it is seen that when the bubble is positioned near the center of the 1D sound field, where the sum of buoyancy and Bjerknes forces vanishes, the buoyancy is largest and the collapse radius is smallest, as the bubble sees the increased driving pressure at the center of the standing wave and responds with highly nonlinear oscillations. The situation complicates when multifrequency driving is employed.

The Gilmore model [14] describing the radial motion of an argon bubble in water is integrated numerically,

$$\left(1-\frac{\dot{R}}{C}\right)R\ddot{R}+\frac{3}{2}\left(1-\frac{\dot{R}}{3C}\right)\dot{R}^2=\left(1+\frac{\dot{R}}{C}\right)H+\left(1-\frac{\dot{R}}{C}\right)\frac{R}{C}\frac{dH}{dt}, \tag{4}$$

$$H=\int_{p\infty}^{p(R)}\rho^{-1}dp, \quad \frac{p+B}{p_0+B}=\left\{\frac{\rho}{\rho_0}\right\}^n,$$

$$C=c|_{r=R}=\sqrt{\left.\frac{dp}{d\rho}\right|_{r=R}}=c_0\left(\frac{p(R,\dot{R})+B}{p_0+B}\right)^{(n-1)/2n},$$

$$p(R,\dot{R})=\left(p_0+\frac{2\sigma}{R_0}\right)\left(\frac{R_0^3-a^3}{R^3-a^3}\right)^{\kappa}-\frac{2\sigma}{R}-\frac{4\mu}{R}\dot{R}. \tag{5}$$

Here R is the bubble radius; C, ρ, and p are the speed of sound in the liquid, its density, and the pressure at the bubble wall, respectively. H is the enthalpy of the liquid. Parameters were set to $c_0=1483$ m/s, $\sigma=0.0725$ N/m, and $\mu=0.001$ Ns/m^2. $a=R_0/8.86$ is a hard-core van der Waals term [15] and κ a polytropic exponent. Its value is set between 1 (=isothermal) and 5/3 (adiabatic collapse) for a monoatomic gas such as argon [16] according to an instantaneous Peclet number reflecting the thermal conduction at the involved time scales. The Tait equation is taken as the equation of state for water using $n=7.025$, $B=3046$ bars [13] as parameters.

The pressure at infinity is $p_\infty=p_0+p_e(z,t)$, with the ambient pressure p_0 and the spatially dependent driving pressure field

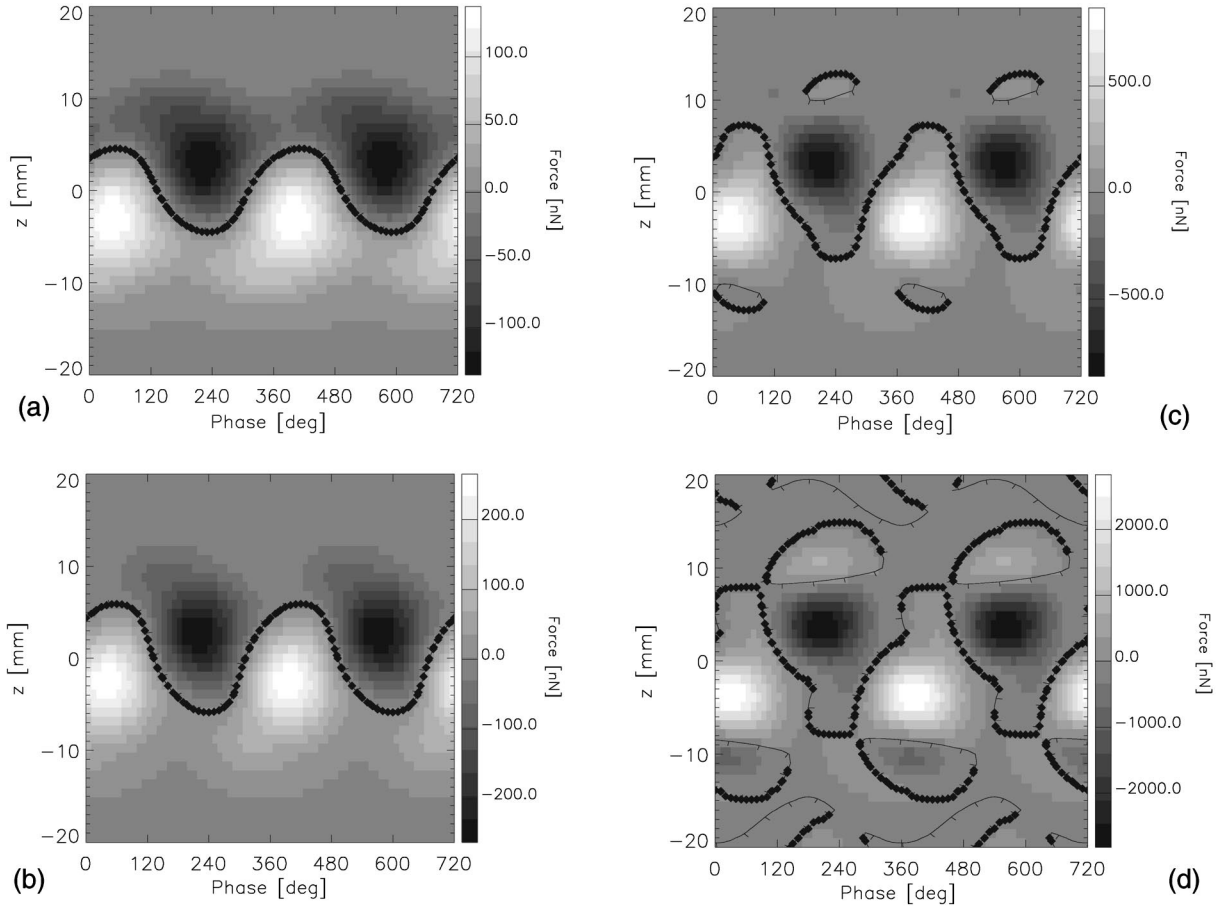

FIG. 3. Bjerknes and buoyancy forces on a bubble driven by a two-frequency sound field consisting of first and second harmonic. Stable and unstable positions of the bubble are shown as a function of temporal phase difference between both driving components. The driving pressure of the first harmonic ($f=23.4$ kHz) is 1.4 bars and the pressure of the second harmonic ($f=46.8$ kHz) is (from top to bottom) (a) 0.07, (b) 0.14, (c) 0.35, (d) 0.7 bars. The phase difference of the spatial modes is −90°.

$$p_e(z,t) = p_{e,1}\cos(\omega_1 t)\cos(k_1 z) + p_{e,2} \times \cos(\omega_2 t + \phi_t)\cos(k_2 z + \phi_z). \quad (6)$$

The values for the first contribution, the first harmonic, follow Eq. (3). The second contribution for the added harmonic has $\omega_2 = 2\pi n f$, $n=2,3,\ldots$, and the wave number $k_2 = 2\pi/\lambda_2$, λ_2 being the wavelength. A spatial phase shift ϕ_z and a temporal phase shift ϕ_t are introduced in the definition for the added harmonic to attribute for a spatial shift in the phase of the standing wave as observed in experiments and to use the temporal phase as a parameter.

III. NUMERICAL RESULTS

A. General remarks

In the numerical examples Secs. III B–III E an argon bubble [17] of 4 μm fixed ambient radius is used unless otherwise noted. The main driving frequency (first harmonic) is 23.4 kHz, the same as in our experiments [5,10,13]. The bubble model [Eq. (4)] is integrated using a specified driving form consisting of the sum of two frequencies. The bubble is placed in z space (parallel to the gravity vector) and the resulting Bjerknes (1) and buoyancy (2) forces are calculated.

Gray scale diagrams are shown that encode the sum of both forces. More negative forces are encoded darker. Contour lines are drawn in the gray scale diagram denoting that the sum of forces is zero. Small lines attached to the zero-force lines point the direction of negative forces. Positive forces are shifting the bubble upwards in space (positive z). The stable positions are shown by filled symbols on the zero-force lines. In the calculations with a fixed ambient radius a high energetic collapse is expressed by a small minimum radius.

In Sec. III F calculations for a bubble in degassed water of a fixed concentration of dissolved air are presented. The number and type of molecules in the bubble ($\propto$ ambient radius) adjust themselves along with the position of the bubble in the sound field, which is also modeled.

B. Dependence on spatial phase

In Fig. 2 examples of biharmonic drivings utilizing a first and second harmonic are shown. As a function of the temporal phase difference the sum of forces and zero-force lines

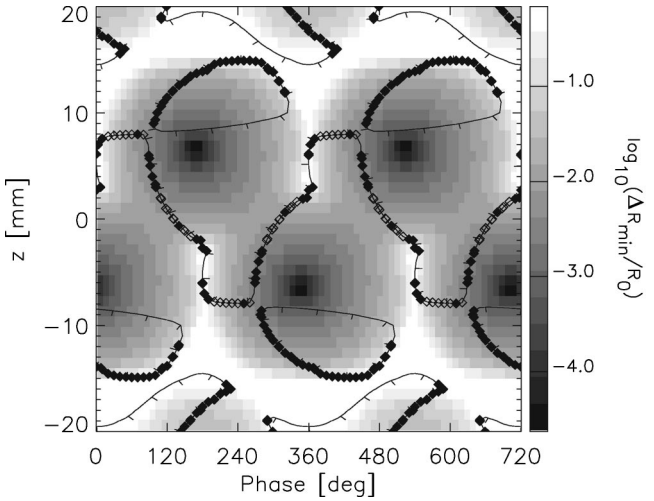

FIG. 4. Minimum radius at bubble collapse. The difference of the collapse radius to a global minimum is encoded by a logarithmic gray scale. Same data as in Fig. 3(d) except the ambient radius that is 4.25 μm. The vanishing sum of Bjerknes and buoyancy forces defines the stability lines of the bubble. Parametrically unstable bubbles have opaque symbols.

are shown. Stable positions of the bubble are denoted by filled symbols on the zero-force lines. Figures 2(a)–2(c) have different values of the spatial phase [Eq. (6)].

Multiple zero-force lines are seen. Coexisting spatially stable and also unstable regions can be determined as well as islands with stable/unstable boundaries. They originate in saddle-node bifurcation points. On the unstable line the sum of Bjerknes and buoyancy forces vanishes, but slight perturbations of the position move the bubble to one of the two nearest stable positions. The figures are almost symmetric around the $z=0$ line; however, the only symmetry breaking effect present is the buoyancy force. Large spatial oscillations by varying the temporal phase difference are seen for all spatial phase differences between modes. Figure 2(d) shows the minimal radii during collapse for the different parameter values of Figs. 2(a)–2(c). Large fluctuation are seen. At some values of the temporal phase difference, the bubble hardly oscillates, as the radius during collapse almost equals the ambient radius. However, a broad plateau exists in the range of values of the temporal phase, where the bubble is oscillating violently. The absolute minimum of the collapse radius is almost at the same temporal phase for all spatial phases.

C. Dependence on amplitudes

The positional stability lines of a bubble in a bimodal driving field depend on the amplitude of the second added frequency. Figure 3 shows the results of the sum of forces on a 4 μm bubble and the stability lines at different pressures. While the amplitude of the first harmonic is fixed at 1.4 bars, the pressure of the second harmonic is varied in four steps from 0.07 to 0.7 bars. The large oscillations of the stable bubble position as a function of the temporal phase are seen. Their amplitudes increase with increasing second harmonic

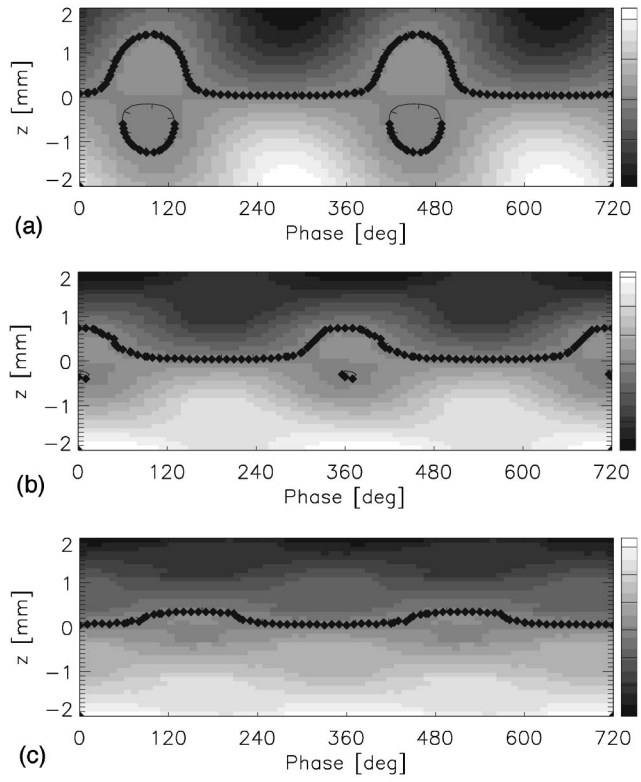

FIG. 5. Bjerknes forces and equilibrium positions as function of temporal phase shift between the two driving components of a bubble undergoing very high frequency harmonic $f+nf$ driving, $f=23.4$ kHz: (a) $n=10$, (b) $n=20$, (c) $n=40$. The driving amplitudes are 1.4 bars for f and 0.07 bars for the nf component.

driving pressure. At 0.35 bars pressure the zero-force lines surround small islands in the force landscape. Also, lines showing spatially unstable bubble behavior are seen. The complexity increases at 0.7 bars where multiple coexisting stability lines are present with unstable connections. A bubble can oscillate stably along the stability lines marked by filled symbols and would sometimes jump by a discrete amount if the temporal phase is changed. Figure 4 shows results for a bubble of 4.25 μm ambient radius. Different collapse radii as a function of position and phase difference are shown together with the stability lines. It is seen that the collapse radius changes along the stability lines. Bjerknes and buoyancy forces keep the bubble away from regions with a very high energetic collapse.

In the multiple stability regime the different bubble positions are associated with vastly different dynamics. While at some points the bubble hardly oscillates others show enormous compression ratios needed for sonoluminescence. Also shown are parametrically (surface) unstable bubbles [18]. Bubbles driven at these phases/positions will show a dancing behavior with less radial compression.

D. Very high frequency modes

When the added harmonic's frequency is a very high multiple of the main driving frequency, it is seen that the bubble still responds to relative phase changes between both driving

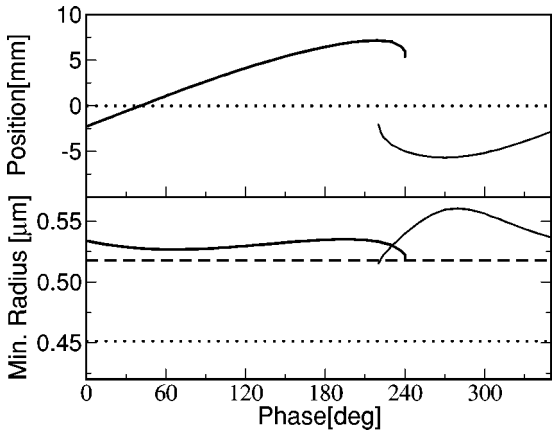

FIG. 6. Stable and unstable equilibrium positions of a bubble undergoing 2f driving $f_2=2f_1$ as a function of temporal phase difference. The second harmonic is a running wave (no spatial mode). The pressures are $p_1=1.4$ bars and $p_2=0.07$ bars. Top: position, bottom: minimum radius at collapse time. Dashed line denotes minimum radius with same power $1f$ driving; the lower line is van der Waals hard core.

components (Fig. 5). The second frequency is changed as nf, $n=10$, 20, 40; $f=23.4$ kHz. Figure 5 shows the Bjerknes and buoyancy forces and the stable positions of a bubble with ambient radius of 4 μm as a function of temporal phase difference. The spatial phase shift is 0°. Figure 5(a) corresponds to Fig. 2(a) where two almost symmetric stability lines exist, whose symmetry is broken due to buoyancy. With increasing order of the added harmonic a change in response is seen: the phase interval during which the position changes shrinks at high frequency. When the $40f$ harmonic is added to the driving, the bubble almost digitally switches between an upper and lower position. This may be attributed to the increased interaction of the harmonic with the afterbounce frequency which is almost equal to the linear resonance frequency of the 4 μm bubble [19]. The radial dynamics, i.e., the minimum radius at collapse is not affected by adding very high harmonics.

E. Running waves

The position of a bubble in a sound field is not only determined by standing waves or spatial modes but also by the eventually present running waves. In Ref. [20] higher harmonics of the driving have been measured; some of them behaved like running waves with no apparent spatial mode. In Fig. 6 an upward pointing running wave of second harmonic frequency ($p=0.07$ bars) is added to the main driving component ($p=1.4$ bars) which has a fixed spatial mode [Eq. (3)]. As a function of temporal phase difference large oscillations are seen. Also a region showing a bistable behavior with an unstable branch of stability lines is seen (saddle-node bifurcation). The bottom part of Fig. 6 shows that the minimum radius at collapse is oscillating near the minimum radius of a $1f$ driving with the same power. The $1f$ driven bubble is located 84 μm above the antinode where the sound pressure is 1.2 Pa less than the maximum.

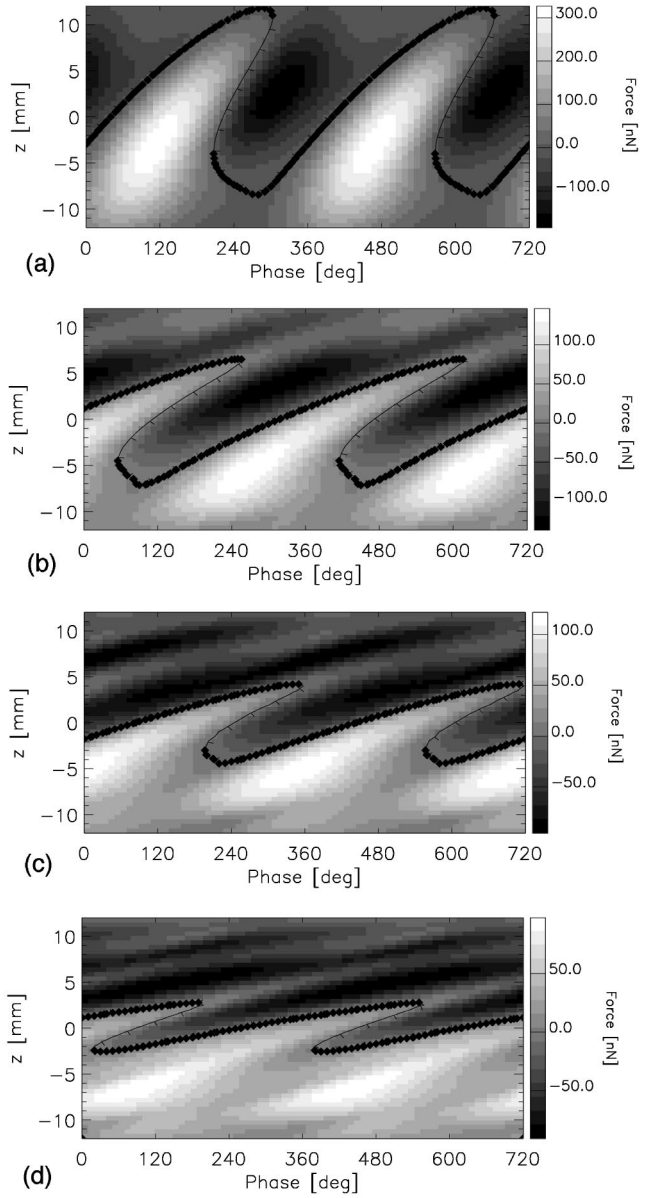

FIG. 7. Stable (filled symbols) and unstable equilibrium positions of a bubble driven by a two-frequency signal as a function of temporal phase difference. The first harmonic is a standing wave mode. The added nth harmonic is a running wave (no spatial mode). The sum of Bjerknes and buoyancy forces is encoded by a gray scale. The pressures are $p_1=1.4$ bars and $p_n=0.14$ bars the frequencies are; $f_1=23.4$ kHz, $f_n=nf_1$, $n=2,5,7,10$ (a–d).

In Fig. 7 the dependence of the positional changes on the frequency of the running wave is seen. Bjerknes force, buoyancy force, and stability lines are shown for added frequencies up to the tenth harmonic. Generally speaking, the amplitudes of the spatial variations decrease with increasing frequency. The bistable regions, however, increase in the parameter space of the spatial phase.

F. Diffusion and dissociation

The results so far are calculated for a bubble with a fixed equilibrium radius. In experimental situations, where a

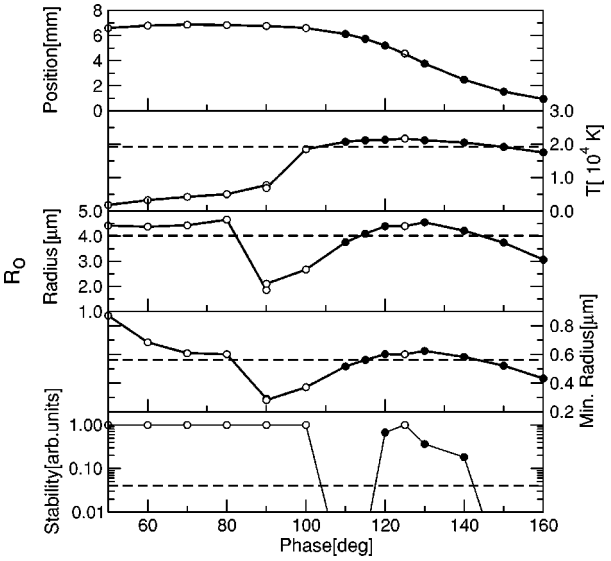

FIG. 8. Changes of bubble behavior when driven by a biharmonic ($f+2f$) signal. The equilibrium radius is allowed to dynamically adjust using a model for diffusion and dissociation of dissolved air in the water. The saturation level is set to 30%. The pressures are $p_1=1.24$ bars and $p_2=0.29$ bars, the frequencies are $f_1=23.4$ kHz and its second harmonic. Shown are (top to bottom) (a) bubble position, (b) temperature at main collapse, (c) ambient radius, (d) minimum radius at collapse, (e) parametric stability as a function of the phase difference between driving components. Parametrically stable bubbles are shown with opaque circles. The dashed lines show results for single-frequency forcing with $p=1.3$ bars, which is the maximal driving pressure for a diffusionally and parametrically stable bubble at this saturation level.

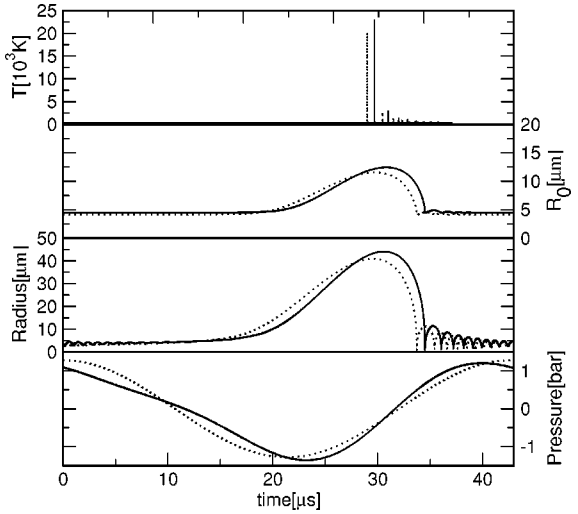

FIG. 9. Time series of bubble dynamics: Comparison between single-frequency (dashed line) and biharmonic (straight line) driving of a bubble. The results represent a parametrically, diffusionally, and translationally stable bubble with maximum driving. The same parameters as in Fig. 8 have been used, except the single-frequency driving pressure that is 1.28 bars. The phase difference of the biharmonic driving is 112°. The bubble model includes evaporation and condensation of water molecules. Shown are the temperature, ambient radius, bubble wall radius, and driving pressure as a function of time.

bubble is levitated in water in which air molecules are dissolved with a fixed saturation level, the number of molecules and their individual partial pressures in the bubble will dynamically adjust when other parameters are changed. The minimal radius, which is a measure for the intensity of a fixed sized bubble's collapse, is now also a function of the dynamics. To measure the intensity of a collapse, the temperature within the bubble is calculated.

The bubble model is extended [21] to include diffusion of dissolved gases in water (N_2, O_2, Ar) [22], chemical dissociation of molecules [16,23], continuous adjustment of the van der Waals hard core, thermal diffusion by smooth isothermal/adiabatic switching during the compression/expansion phase [16], and 1D spatial bubble translation with variable damping according to the Reynold's number and parametric stability [18]. During the calculations a bubble is allowed to dynamically evolve over many cycles into a diffusional and spatial equilibrium starting from specified initial conditions.

In Fig. 8 the behavior of a bubble in water of a fixed saturation level of 30% is shown. The dashed line shows the values obtained for single-frequency driving at 1.3 bars, the maximal driving pressure above which the bubble is parametrically unstable. The values for the parametric stability are shown in Fig. 8(e). Values exceeding 1 denote an unstable bubble where surface oscillations lead to a breakup. As seen in experiments [1,13], the bubble tends to "dance," whereby it cycles through a process set up by rectified diffusion and subsequent microbubble splitoff. In Fig. 8, transparent symbols denote results for cycling bubbles just crossing the stability (=1) line.

Calculations are made for a biharmonic driving of first and second harmonic with phase differences from 0 to 180°: Below 50° and from 160°–180° phase difference a bubble dissolves on a slow time scale. From 50°–80° the bubble is relatively cold [Fig. 8(b)]. It is growing by rectified diffusion, is not able to dissociate much of its contents, and contains mostly air. The growth is limited by the parametric stability threshold. At 90° chemical dissociation of N_2 and O_2 sets in as seen in the decrease of the ambient radius [Fig. 8(c)]. The two symbols show results for a (diffusively unstable) argon bubble developing into the final bubble containing some gas mixture. Bubbles between 110° and 160° have a hot collapse phase, consist solely of argon, and are stable, with the exception of a small island around 125°. The hottest stable bubble is produced by a phase difference of 120°, where it reaches 21 600 K (compare to 19 200 K for the monofrequent driving). The bubble driven using a phase difference in this regime has a consistently hotter collapse as when using $1f$ driving. Also, the $2f$-driven bubble is bigger during collapse, leading to a larger radiating volume. These numerical results can be compared to the experimental results in Ref. [5], where the spatial translations, excess light emission, and parametric instabilities are also published.

A further extension of the model [21] to include water vapor evaporation and condensation [24,25] is leading to the results of Fig. 9. The amplitude of the monofrequent and the relative phase of the bifrequent driving signal have been cho-

sen, such that maximum temperature at collapse is attained, whereby maintaining diffusional, translational, and parametric stability. The maximum temperatures are higher than in the previous calculations, an effect that is due to the larger extent of the bubble's maximum radius obviously compensating the temperature lowering effect of a smaller polytropic exponent of the bubble's interior at collapse. Again, the biharmonic driving produces a hotter bubble (23 000 K vs 20 000 K) with a larger radius at collapse (radiating volume) (0.61 μm vs 0.57 μm). The temperature pulse duration is slightly longer for the biharmonic driving.

IV. DISCUSSION

Biharmonic drivings of bubbles show a variety of effects. While the bubble's own nonlinearity interacts with the more complex sound field, as compared to single-frequency driving, changes in cavitation and sonoluminescence intensity are observed. The position of the bubble adjusts itself in the sound field, where the sum of the Bjerknes force and the buoyancy force vanishes. The effects depend on the adjustment of the relative phases between the two-frequency components of the driving signal. While the spatial modes are more or less fixed with a given experimental setup, the temporal phase difference between two harmonics can be easily adjusted. By varying this difference the positional changes of the bubble as well as its collapse intensity are controllable. The dependence on a number of parameters has been shown. By increasing the amplitude of the added harmonic, complex lines appear in the levitation space as a function of temporal phase difference. They identify spots where a bubble can be stably positioned. Unstable zero-force lines appear, where the sum of forces is negative but where small disturbances make the bubble visit other stable regions. Multiple stability lines appear showing that a bubble can be positioned in more than one spot in this sound field. The stable and unstable lines are connected by saddle-node bifurcation points. Also disconnected islands appear showing that discrete jumping of bubbles to different spots in a levitation cell is possible.

By varying the spatial phase between the modes (standing waves) in a one-dimensional levitation setup, it is seen that, as a function of the temporal phase, different levitation lines appear. Regardless of the spatial phase, the most energetic collapse is around 115° of the temporal phase difference. The least energetic collapses for the different spatial phase shifts are at different values of the temporal phase shifts. Position shifts are observed for all adjustments of the spatial phase difference of two modes.

All calculations for 4μm ambient radius show results for a positionally and parametrically stable bubble. As the parameter space for sonoluminescence [26] requires the water to be degassed, the low energetic collapses observed in the diagrams will probably make a bubble disappear due to diffusion [7]. The diffusion will change the ambient radius of the bubbles at different drivings. At higher gas levels the ambient radius of a bubble might grow to an extent, where the bubble will become unstable to surface mode oscillations. In an experimental situation one has to adjust the ambient gas concentration in order to get a stable bubble of a certain radius. A more complex model also allowing for diffusional changes in the number and type of molecules in a bubble is integrated. These calculations for a bubble in degassed water with a fixed concentration of dissolved air show that the control of the dynamics allows for higher or lesser temperatures at collapse or also removal of bubbles. Sonoluminescing bubbles can be levitated at specified spots in the cell by micromanipulation due to biharmonic drivings. Targeting shock waves to drive a bubble may be feasible with the method described here.

Biharmonic excitations might be of use in attempts to control cavitation. By careful choice of phase differences a violent collapse can also be inhibited. The injection of a phase stabilized harmonic can be used for the generation of a multibubble cavitation system, where the destruction of streamer patterns is possible to reduce metal abrasion and to enhance overall cleaning capabilities of acoustic cavitation. Inertial bubble growth of microbubbles could be controlled by the use of an adapted biharmonic signal.

V. CONCLUSION

We have shown the effects on spatial and temporal bubble dynamics when a bubble is driven in a biharmonic sound field. The parameter dependences include amplitudes of higher harmonics, spatial and temporal phase, standing waves/modes and running waves, and the effects of very high harmonics. The effects of gas diffusion through the bubble wall, chemical dissociation of gas species, and water vapor under parametrical and spatial stability conditions have been shown. The results may serve as a tool for the experimental control and micromanipulation of sonoluminescing bubbles and multibubble cavitation.

ACKNOWLEDGMENTS

The authors thank R. G. Holt and D. F. Gaitan for stimulating discussions. Part of this work was funded by the SFB 185 "Nichtlineare Dynamik" of the DFG.

[1] D. F. Gaitan, L. A. Crum, C. C. Church, and R. A. Roy, J. Acoust. Soc. Am. **91**, 3166 (1992).
[2] B. P. Barber and S. J. Putterman, Nature (London) **352**, 318 (1991); B. P. Barber, R. A. Hiller, R. Löffstedt, S. J. Putterman, and K. R. Weninger, Phys. Rep. **281**, 65 (1997).
[3] R. Pecha, B. Gompf, G. Nick, Z. Q. Wang, and W. Eisenmenger, Phys. Rev. Lett. **81**, 717 (1998).
[4] F. B. Seeley, J. Acoust. Soc. Am. **105**, 2236 (1999).
[5] J. Holzfuss, M. Rüggeberg, and R. Mettin, Phys. Rev. Lett. **81**, 1961 (1998).
[6] K. Hargraeves and T. J. Matula, J. Acoust. Soc. Am. **107**, 1774 (2000).

[7] J. A. Ketterling and R. E. Apfel, J. Acoust. Soc. Am. **106**, 2290 (1999).
[8] F. J. Moraga, R. P. Taleyarkhan, R. T. Lahey, and F. J. Bonetto, Phys. Rev. E **62**, 2233 (2000).
[9] M. Rüggeberg and J. Holzfuss, *Fortschritte der Akustik - DAGA* (DPG GmbH, Bad Honnef, 2000), pp. 772 and 773.
[10] M. Rüggeberg, *Stoßwellenemission und die akustische Umgebung einer sonolumineszierenden Blase* (Shaker,Aachen, 2000).
[11] W. C. Moss, D. B. Clarke, J. W. White, and D. A. Young, Phys. Lett. A **211**, 69 (1996).
[12] J.-L. Thomas, Y. Forterre, and M. Fink, Phys. Rev. Lett. **88**, 074302 (2002).
[13] J. Holzfuss, M. Rüggeberg, and A. Billo, Phys. Rev. Lett. **81**, 5434 (1998).
[14] F. R. Gilmore, California Institute of Technology Report No. 26-4, 1952 (unpublished).
[15] R. Löffstedt, B. P. Barber, and S. J. Putterman, Phys. Fluids A **5**, 2911 (1993).
[16] D. Lohse, M. P. Brenner, T. F. Dupont, S. Hilgenfeldt, and B. Johnston, Phys. Rev. Lett. **78**, 1359 (1997).
[17] B. P. Barber, K. Weninger, R. Löfstedt, and S. Putterman, Phys. Rev. Lett. **74**, 5276 (1995); J. A. Ketterling and R. E. Apfel, *ibid.* **81**, 4991 (1998); T. J. Matula and L. A. Crum, *ibid.* **80**, 865 (1998).
[18] M. P. Brenner, D. Lohse, and T. F. Dupont, Phys. Rev. Lett. **75**, 954 (1995).
[19] T. G. Leighton, *The Acoustic Bubble* (Academic Press, London, 1994).
[20] J. Holzfuss, M. Rüggeberg, and R. G. Holt, Phys. Rev. E **66**, 046630 (2002).
[21] J. Holzfuss and M. Rüggeberg (unpublished).
[22] M. M. Fyrillas and A. J. Szeri, J. Fluid Mech. **277**, 381 (1994).
[23] M. P. Brenner, S. Hilgenfeldt, and D. Lohse, Rev. Mod. Phys. **74**, 425 (2002).
[24] R. Toegel, B. Gompf, R. Pecha, and D. Lohse, Phys. Rev. Lett. **85**, 3165 (2000).
[25] K. Yasui, J. Phys. Soc. Jpn. **66**, 2911 (1997).
[26] R. G. Holt and D. F. Gaitan, Phys. Rev. Lett. **77**, 3791 (1996); D. F. Gaitan and R. G. Holt, Phys. Rev. E **59**, 5495 (1999).